Chapter 2
Modeling of Low-Dimensional Semiconductors

Hilmi Ünlü, H. Hakan Gürel, Özden Akıncı, and Mohamed Rezaul Karim

Abstract In this chapter, we discuss the general methodology to carry out qualitatively reliable and quantitatively precise calculations of electronic band structure of heterostructures that are essential in the realistic modeling and prediction of device performance in technologically important semiconductor devices, which can proceed relatively independently of experiment.

2.1 Introduction

Realization of the full potential of low-dimensional semiconductor structures for making bipolar and unipolar electronic devices (such as heterostructure bipolar transistors (HBTs) and modulation-doped field effect transistors (MODFETs)) and optical devices (including heterostructure lasers and light-emitting diodes) requires a reliable, precise predictive process and performance simulation models based on the fundamental principles of solid-state physics and quantum mechanics. Among the key issues are the understanding of the formation and determination of the magnitude of conduction and valence band offsets at heterointerfaces, which dominate various device properties such as injection efficiency in HBTs and carrier confinement in MODFETs. These issues have received considerable attention among device scientists and engineers over the years [1, 2].

The use of low-dimensional semiconductor structures in device design enables device engineers to locally modify the energy band structure of the constituents

H. Ünlü (✉)
Computational Science Division, Informatics Institute, Istanbul Technical University, Maslak Istanbul 80626, Turkey

Department of Physics, Faculty of Science and Letters, Istanbul Technical University, Maslak Istanbul 80626, Turkey
e-mail: hunlu@itu.edu.tr; hilmi.unlu74@gmail.com

H. Ünlü and N.J.M. Horing (eds.), *Low Dimensional Semiconductor Structures*, NanoScience and Technology, DOI 10.1007/978-3-642-28424-3_2,

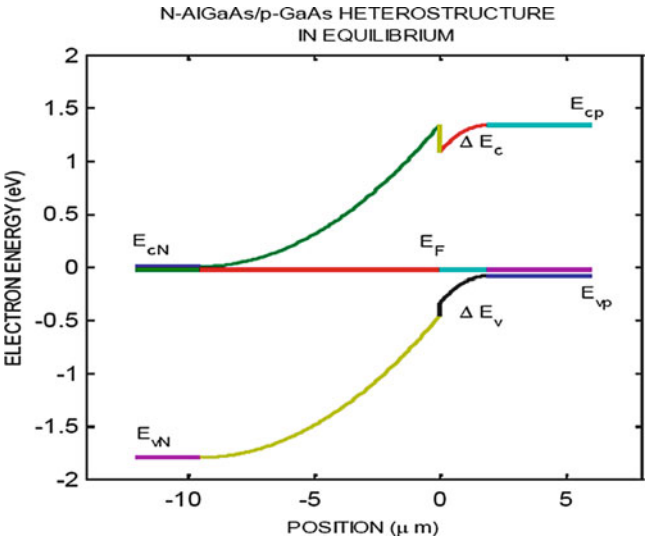

Fig. 2.1 Schematic energy band diagram of an n-AlGaAs/p-GaAs heterojunction in thermal equilibrium. When the semiconductor composition changes abruptly at the interface between constituents, the difference in their energy bands is accommodated by discontinuities in the conduction and valence bands

in order to control the motion of charge carriers [3, 4]. When two semiconductors having different physical and chemical properties and thicknesses are grown upon each other, the lattice mismatch and thermal expansion gradient at the growth temperature gives rise to interface strain that modifies the electronic properties of both materials near the interface, including the band offsets (as shown in Fig. 2.1 for an n-AlGaAs/p-GaAs heterojunction in thermal equilibrium) and consequently the energy profile experienced by moving charge carriers at the conduction and valence band edges. This facilitates the control of device performance [2–10].

In this chapter, we discuss the general methodology to carry out qualitatively reliable and quantitatively precise calculations of electronic band structure of heterostructures that are essential in the realistic modeling and prediction of device performance in technologically important semiconductor devices, which can proceed relatively independently of experiment. The models we shall discuss in this chapter are (1) the semiempirical sp^3 tight-binding (TB) theory in comparison with (2) density functional theory (DFT) of band structure modeling, which can be very easily implemented in extended current transport modeling in low-dimensional semiconductor structures.

When a wide-gap semiconductor is grown on a narrow-gap semiconductor base, the interface strain, caused by the lattice mismatch, modifies the structural and electronic properties of the constituent semiconductors in directions parallel and perpendicular to the interface [1]. The macroscopic observable consequences of lattice mismatch and thermal strains are the change in the bandgap, effective mass,

intrinsic carrier density, and dielectric constant as a function of temperature. The interface strain splits the heavy-hole, light-hole, and split-off valence band edges by its uniaxial component and shifts the position of the conduction and valence band edges, and the hydrostatic strain component alters the magnitude of the energy levels of the constituent semiconductors [11], as shown in Fig. 1.1. The positions of the heavy-hole, light-hole, and split-off valence band energies relative to the average valence band edge E_v are given by the following equations:

$$E_{vh}(\varepsilon) = E_v(\varepsilon) + \frac{1}{3}\Delta - \frac{1}{2}\delta E \tag{2.1}$$

$$E_{vl}(\varepsilon) = E_v(\varepsilon) - \frac{1}{6}\Delta + \frac{1}{4}\delta E + \frac{1}{2}\sqrt{\Delta^2 + \Delta\,\delta E + \frac{9}{4}\delta E^2} \tag{2.2}$$

$$E_{vs}(\varepsilon) = E_v(\varepsilon) - \frac{1}{6}\Delta + \frac{1}{4}\delta E - \frac{1}{2}\sqrt{\Delta^2 + \Delta\delta E + \frac{9}{4}\delta E^2} \tag{2.3}$$

where $\delta E = 2b(\varepsilon_{zz} - \varepsilon_{xx}) = 2b(\varepsilon_{\perp} - \varepsilon_{\parallel})$ and b is the shear deformation potential that describes the splitting in the valence band energy due to the [001] uniaxial strain. $E_v(\varepsilon)$ is the average valence band maximum that is under the hydrostatic component of the biaxial strain. $E_{vh}(\varepsilon)$ is the heavy-hole band, $E_{vl}(\varepsilon)$ is the light-hole band, and $E_{vs}(\varepsilon)$ is the split of band defined with respect to average valence band maximum.

Compressive or tensile strain (($\varepsilon_{xx} < 0$) or ($\varepsilon_{xx} > 0$)) on the epilayer results in an increase or decrease in its conduction and valence band energy levels (Fig. 2.2). Therefore, any interface strain will modify the band offsets that determine carrier transport across the interface of electronic or optical devices. Reliable and precise determination of the effects of strain on the electronic band structure is essential for the reliable design and precise performance predictions of HBTs as high speed, high power, and low noise bipolar transistors. In the following subsections, temperature, pressure, strain, and alloy composition effects on energy bandgaps and band offsets will be discussed by using the sp^3 TB theory of semiconductors [12–20].

Quantitatively reliable and numerically precise modeling and simulation of electronic properties of compound semiconductors and their ternary alloys permits better prediction of their material properties [12–20]. First-principles calculations are known to be computationally intensive and cannot be easily implemented for some optoelectronic devices [10]. In contrast, the semiempirical TB model is known to be not only simple but also reliable and easily implemented, and has great advantages over first-principles calculations in determining electronic properties such as band structure, density of states (DOS), and bandgaps of low-dimensional semiconductor structures. The semiempirical TB model is an atomistic approach and well suited to calculate the electronic band structure of low-dimensional semiconductor structures, including quantum wells and quantum dots [10]. In the following section, we discuss the use of second nearest neighbor (2NN) sp^3s^* [21] and nearest neighbor (NN) $sp^3d^5s^*$ [22, 23] TB models to calculate the composition, temperature, pressure, and strain effects on electronic properties (e.g.,

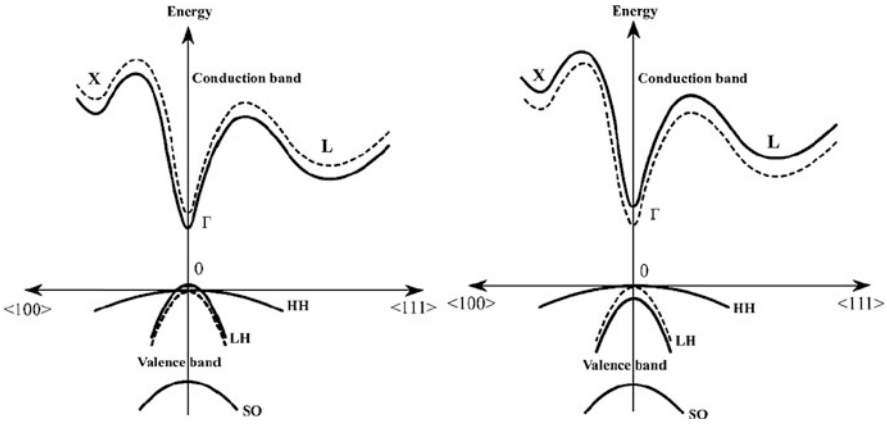

Fig. 2.2 The tensile strain ($\varepsilon_{xx} > 0$) (on *left*) results in the modification of the semiconductor energy band structure (e.g., bandgap decreases). On the other hand, compressive strain ($\varepsilon_{xx} < 0$) (on *right*) results in the modification of semiconductor energy band structure (e.g., bandgap increases). *HH*, *LH*, and *SO*, respectively, represent the heavy-hole, light-hole, and split-off band energies

band structure, DOS, bandgaps, and band widths) of semiconductor binaries and their ternaries.

2.2 TB View of Semiconductor Structures

Within the framework of Slater–Koster-type semiempirical sp^3 TB theory [24–26], one first writes the Schrodinger equation in matrix form as

$$\sum_{\beta} \left[H_{\alpha\beta}(k) - S_{\alpha\beta}(k) E \right] u_{\beta} = 0, \tag{2.4}$$

where E is the energy eigenvalue of the 10×10 Hamiltonian matrix $H_{\alpha\beta} = \langle \chi_{\alpha}(k) | H | \chi_{\beta}(k) \rangle$ and $S_{\alpha\beta} = \langle \chi_{\alpha}(k) | \chi_{\beta}(k) \rangle$ is the overlap integral between the atomic-like orbitals, with α and β that correspond to cation (c) and anion (a) s(p) atomic orbitals, respectively. $\chi(k)$ is the basis function formed by the linear combination of cation and anion s(p) atomic orbitals and u_{β} is the wave function coefficient. Considering a compound semiconductor having a zinc blende crystal structure, shown in Fig. 2.3, the interaction between s^a ile s^c orbits is written as

$$\langle s^c | H | s^a \rangle = E_{ss} \sum_{n=1}^{4} e^{ik.r_n} = E_{ss} \left(e^{ik.r_1} + e^{ik.r_2} + e^{ik.r_3} + e^{ik.r_4} \right) \tag{2.5}$$

where

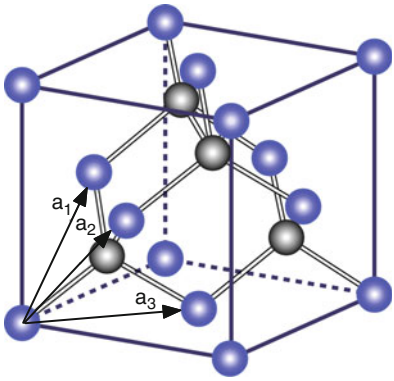

Fig. 2.3 Unit cell of zinc blende crystal structure

$$
\begin{aligned}
r_1 &= (a/4)(+1,+1,+1),\\
r_2 &= (a/4)(+1,-1,-1),\\
r_3 &= (a/4)(-1,+1,-1),\\
r_4 &= (a/4)(-1,-1,+1)
\end{aligned}
$$

are the displacement vectors of NNs. The interaction between the s, p_x, p_y, p_z orbitals of the first cation atom and second NN anion atoms can be described by the following integral expressions:

$$\langle s^c|H|s^a\rangle = E_{ss}\left(e^{ik,r_1} + e^{ik,r_2} + e^{ik,r_3} + e^{ik,r_4}\right) = E_{ss}B_0(k), \tag{2.6}$$

$$\langle s^c|H|p_x^a\rangle = E_{sp}\left(e^{ik,r_1} + e^{ik,r_2} + e^{ik,r_3} + e^{ik,r_4}\right) = E_{sp}B_1(k), \tag{2.7}$$

$$\langle s^c|H|p_y^a\rangle = E_{sp}\left(e^{ik,r_1} + e^{ik,r_2} + e^{ik,r_3} + e^{ik,r_4}\right) = E_{sp}B_2(k), \tag{2.8}$$

$$\langle s^c|H|p_z^a\rangle = E_{sp}\left(e^{ik,r_1} + e^{ik,r_2} + e^{ik,r_3} + e^{ik,r_4}\right) = E_{sp}B_3(k). \tag{2.9}$$

The interactions between the same p-orbitals of cation and anion atoms are called diagonal matrix elements and are calculated by the following integral expressions:

$$\langle p_x^c|H|p_x^a\rangle = E_{xx}B_0(k), \tag{2.10}$$

$$\langle p_y^c|H|p_y^a\rangle = E_{xx}B_0(k), \tag{2.11}$$

$$\langle p_z^c|H|p_z^a\rangle = E_{xx}B_0(k). \tag{2.12}$$

The interactions between different p-orbitals of cation and anion atoms are called off-diagonal matrix elements and are calculated by the following integral expressions:

$$\langle p_x^c|H|p_y^a\rangle = \langle p_y^c|H|p_x^a\rangle = E_{xy}B_3(k), \tag{2.13}$$

$$\langle p_x^c|H|p_z^a\rangle = \langle p_z^c|H|p_x^a\rangle = E_{xy}B_2(k), \tag{2.14}$$

$$\langle p_y^c|H|p_z^a\rangle = \langle p_z^c|H|p_y^a\rangle = E_{xy}B_1(k). \tag{2.15}$$

The matrix of semiempirical SP^3 TB Hamiltonian that includes all interaction elements is given by

$$\mathbf{H} = \begin{bmatrix} E_s^c & 0 & 0 & 0 & B_0 E_{ss} & B_1 E_{sp} & B_2 E_{sp} & B_3 E_{sp} \\ 0 & E_p^c & 0 & 0 & -B_1 E_{sp} & B_0 E_{xx} & B_3 E_{xy} & B_2 E_{xy} \\ 0 & 0 & E_p^c & 0 & -B_2 E_{sp} & B_3 E_{xy} & B_0 E_{xx} & B_1 E_{xy} \\ 0 & 0 & 0 & E_p^c & -B_3 E_{sp} & B_2 E_{xy} & B_1 E_{xy} & B_0 E_{xx} \\ B_0^* E_{ss} & -B_1^* E_{sp} & B_2^* E_{sp} & B_3^* E_{sp} & E_s^a & 0 & 0 & 0 \\ B_1^* E_{sp} & B_0^* E_{xx} & B_3^* E_{xy} & B_2^* E_{xy} & 0 & E_p^a & 0 & 0 \\ B_2^* E_{sp} & B_3^* E_{xy} & B_0^* E_{xx} & B_1^* E_{xy} & 0 & 0 & E_p^a & 0 \\ B_3^* E_{sp} & B_2^* E_{xy} & B_1^* E_{xy} & B_0^* E_{xx} & 0 & 0 & 0 & E_p^a \end{bmatrix} \tag{2.16}$$

where $E_{ss}, E_{xx}, E_{s_a p_c}, E_{s_c p_a}, E_{xy}, E_{s^* p}$, and $E_{p s^*}$ are known as hopping terms (transfer matrix elements). The values of $B_0(k)$, $B_1(k)$, $B_2(k)$, and $B_3(k)$ are:

$$\begin{aligned} B_0(k_x, k_y, k_z) &= +4 \cos\left(\frac{k_x a}{2}\right) \cos\left(\frac{k_y a}{2}\right) \cos\left(\frac{k_z a}{2}\right) \\ &\quad -4i \sin\left(\frac{k_x a}{2}\right) \sin\left(\frac{k_y a}{2}\right) \sin\left(\frac{k_z a}{2}\right) \\ B_1(k_x, k_y, k_z) &= +4 \cos\left(\frac{k_x a}{2}\right) \sin\left(\frac{k_y a}{2}\right) \sin\left(\frac{k_z a}{2}\right) \\ &\quad +4i \sin\left(\frac{k_x a}{2}\right) \cos\left(\frac{k_y a}{2}\right) \cos\left(\frac{k_z a}{2}\right) \\ B_2(k_x, k_y, k_z) &= -4 \sin\left(\frac{k_x a}{2}\right) \cos\left(\frac{k_y a}{2}\right) \sin\left(\frac{k_z a}{2}\right) \\ &\quad +4i \sin\left(\frac{k_x a}{2}\right) \sin\left(\frac{k_y a}{2}\right) \cos\left(\frac{k_z a}{2}\right) \\ B_3(k_x, k_y, k_z) &= -4 \sin\left(\frac{k_x a}{2}\right) \sin\left(\frac{k_y a}{2}\right) \cos\left(\frac{k_z a}{2}\right) \\ &\quad -4i \cos\left(\frac{k_x a}{2}\right) \cos\left(\frac{k_y a}{2}\right) \sin\left(\frac{k_z a}{2}\right) \end{aligned} \tag{2.17}$$

where B_i^* is the complex conjugate of B_i matrix element. It should be noted that although the Slater–Koster-type sp^3 TB approach [24–26] yields a good description of valence band dispersion curves, the conduction band dispersion curves are not accurately given, especially the indirect bandgap at the X symmetry point is not well reproduced. In order to overcome this obstacle, Vogl et al. [21] introduced an sp^3s^* TB model in order to include the influence of excited d-states. In this model, each atom is described by not only its outer valence s orbital and three p orbitals but also the fictitious excited s* orbital to take into account the effect of

higher states. The inclusion of spin–orbit coupling of p-states to the sp^3s^* basis set reproduces the splitting between split-off band and the light- and heavy-hole bands. Accounting for 2NN interactions of cation and anion atoms improves the accuracy of the sp^3s^* ETB model in determining the conduction band structure features at X and L high symmetry points. It is possible to accurately calculate the conduction band dispersion curves at the X high symmetry point by adding the excited s* state with spin–orbit coupling to the sp^3s^* orbital basis. Moreover, inclusion of the 2NN interactions of cation and anion atoms in the basis set yields a better fit for the conduction band dispersion curve at the L symmetry point.

2.3 Semiempirical sp^3s^* TB Model

In the semiempirical sp^3s^* TB model Hamiltonian matrix, each cation atom and anion atom are described by their outer valence s orbital, the three outer p orbitals, and a fictitious excited s* orbital added to mimic the effects of higher lying d-states. The inclusion of second (2NN) interactions in the sp^3s^* TB model introduces two additional interaction parameters [10] and the Hamiltonian matrix $H_{\alpha\beta}$ is written as

$$
H_{\alpha\beta} = \begin{bmatrix}
E_s^c & -\varepsilon(s,p_x)B_6 & -\varepsilon(s,p_x)B_5 & -\varepsilon(s,p_x)B_4 & 0 & B_0E_{ss} & B_1E_{sp} & B_2E_{sp} & B_3E_{sp} & 0 \\
-\varepsilon(s,p_x)B_6 & E_p^c & \varepsilon(p_x,p_y)B_4 & \varepsilon(p_x,p_y)B_5 & 0 & -B_1E_{ps} & B_0E_{xx} & B_3E_{xy} & B_2E_{xy} & -B_1E_{ps^*} \\
-\varepsilon(s,p_x)B_5 & \varepsilon(p_x,p_y)B_4 & E_p^c & \varepsilon(p_x,p_y)B_6 & 0 & -B_2E_{ps} & B_3E_{xy} & B_0E_{xx} & B_1E_{xy} & -B_2E_{ps^*} \\
-\varepsilon(s,p_x)B_4 & \varepsilon(p_x,p_y)B_5 & \varepsilon(p_x,p_y)B_6 & E_p^c & 0 & -B_3E_{ps} & B_2E_{xy} & B_1E_{xy} & B_0E_{xx} & -B_3E_{ps^*} \\
0 & 0 & 0 & 0 & E_{s^*}^c & 0 & B_1E_{s^*p} & B_2E_{s^*p} & B_3E_{s^*p} & 0 \\
B_0^*E_{ss} & -B_1^*E_{sp} & -B_2^*E_{sp} & -B_3^*E_{sp} & 0 & E_s^a & \varepsilon(s,p_x)B_6 & \varepsilon(s,p_x)B_5 & \varepsilon(s,p_x)B_4 & 0 \\
B_1^*E_{sp} & B_0^*E_{xx} & B_3^*E_{xy} & B_2^*E_{xy} & 0 & \varepsilon(s,p_x)B_6 & E_p^a & \varepsilon(p_x,p_y)B_4 & \varepsilon(p_x,p_y)B_5 & 0 \\
B_2^*E_{sp} & B_3^*E_{xy} & B_0^*E_{xx} & B_1^*E_{xy} & 0 & \varepsilon(s,p_x)B_5 & \varepsilon(p_x,p_y)B_4 & E_p^a & \varepsilon(p_x,p_y)B_6 & 0 \\
B_3^*E_{sp} & B_2^*E_{xy} & B_1^*E_{xy} & B_0^*E_{xx} & 0 & \varepsilon(s,p_x)B_4 & \varepsilon(p_x,p_y)B_5 & \varepsilon(p_x,p_y)B_6 & E_p^a & 0 \\
0 & -B_1^*E_{ps^*} & -B_2^*E_{ps^*} & -B_3^*E_{ps^*} & 0 & 0 & 0 & 0 & 0 & E_{s^*}^a
\end{bmatrix}
\tag{2.18}
$$

where $E_s^a, E_s^c, E_p^a, E_p^c, E_{s^*}^a$, and E_{s^*c} in $H_{\alpha\beta}$ are known as the on-site atomic energies of cation and anion atoms; $E_{ss}, E_{xx}, E_{s_a p_c}, E_{s_c p_a}, E_{xy}, E_{s^* p}$, and E_{ps^*} are known as hopping terms (transfer matrix elements); and $\varepsilon_{sx} = \varepsilon(sc(a), p_x c(a))$ and $\varepsilon_{xy} = \varepsilon(p_x c(a), p_y c(a))$ are the two 2NN transfer matrix elements for the cation and anion atoms. Here, s and p refer to the basis states, and a and c refer to anion (e.g., As, Sb, and N) and cation (e.g., Al, Ga, and In) atoms, respectively. Here, each cation and anion atoms are described by its outer valence orbitals for each spin: s, p_x, p_y, p_z and an additional s* orbital, which is an excited state of s orbital that accounts for higher lying states. B_0, B_1, B_2, and B_3 are given by (2.17) and others B_4, B_5, and B_6 are written as

$$
\begin{aligned}
B_4(k_x,k_y,k_z) &= 4\sin(k_x a)\sin(k_y a), \\
B_5(k_x,k_y,k_z) &= 4\sin(k_x a)\sin(k_z a), \\
B_6(k_x,k_y,k_z) &= 4\sin(k_y a)\sin(k_z a).
\end{aligned}
$$

Table 2.1 Bandgaps at high symmetry points of GaAs, InAs, GaP, GaN, and InN compounds [28–30] used as input parameters to produce 2NN sp^3s^* TB parameters in Table 2.2

(eV)	GaAs	InAs	GaP	GaN	InN
E_g^{Γ}	1.519	0.430	2.878	3.287	0.872
E_g^{X}	1.980	2.278	2.330	4.691	2.827
E_g^{L}	1.818	1.605	2.563	6.258	3.810

Table 2.2 The 2NN sp^3s^* TB parameters for GaAs, InAs, GaP, GaN, and InN compounds obtained by using the fundamental bandgaps in Table 2.1

(eV)	GaAs	InAs	GaP	GaN	InN
$E_{s,a}$	−8.4399	−9.5381	−8.1124	−12.915	−12.860
$E_{p,a}$	0.9252	0.7733	1.0952	3.1697	1.9800
$E_{s,c}$	−2.6569	−2.7219	−2.1976	−1.5844	−0.3994
$E_{p,c}$	3.5523	3.5834	4.0851	9.0302	8.0200
$E_{s^*,a}$	6.6235	7.2730	8.4796	12.2000	10.6300
$E_{s^*,c}$	7.4249	6.6095	7.1563	12.2000	13.0000
$4V_{s,s}$	−6.4210	−5.6052	−7.4909	−8.8996	−4.2285
$4V_{x,x}$	1.9850	1.8398	2.1516	5.3500	3.9800
$4V_{x,y}$	4.9100	4.3977	5.1213	8.6200	7.4100
$4V_{sa,pc}$	4.2390	3.0205	4.2724	6.4000	3.8100
$4V_{pa,sc}$	5.15358	5.3894	6.3075	7.2400	6.1900
$4V_{s^*a,pc}$	3.80624	3.2191	4.6184	7.0600	6.8800
$4V_{pa,s^*c}$	4.7009	3.7234	5.0534	1.8200	3.3600
ε_{sx}	0.2459	0.1441	0.2325	0.9500	0.6150
ε_{xy}	−0.1050	0.0249	−0.22	1.0100	0.7100
λ_a	0.0553	0.1385	0.0578	0.0035	0.0035
λ_c	0.1338	0.1290	0.0222	0.0410	0.1100

The inclusion of spin–orbit coupling in the sp^3s^* TB model increases the size of the 10×10 Hamiltonian matrix to 20×20 matrix, which is diagonalized for each $\mathbf{k}$ vector to obtain the semiconductor band structure. The spin–orbit effects are included by coupling different spin states of different on-site p orbitals through the spin–orbit interaction. A TB parameterization of the matrix elements for the sp^3s^* 2NN interaction are obtained by fitting the obtained bandgaps given in Table 2.1 to those produced by pseudopotential theory [27], as verified by experimental data [28–30]. The optimized TB parameters are listed in Table 2.2 for GaAs, InAs, GaP, GaN, and InN with cubic crystal structures.

Having reliable diagonal matrix elements allows one to make a realistic TB parametrization of the off-diagonal matrix elements representing the first NN and the 2NN interactions in the calculations of binary and ternary semiconductor electronic band structures. As a first test of the accuracy of the 2NN sp^3s^* TB model, calculated electronic band structures of GaAs and InAs are shown in Fig. 2.4, which exhibit the reproduced conduction and valence band structures, including the

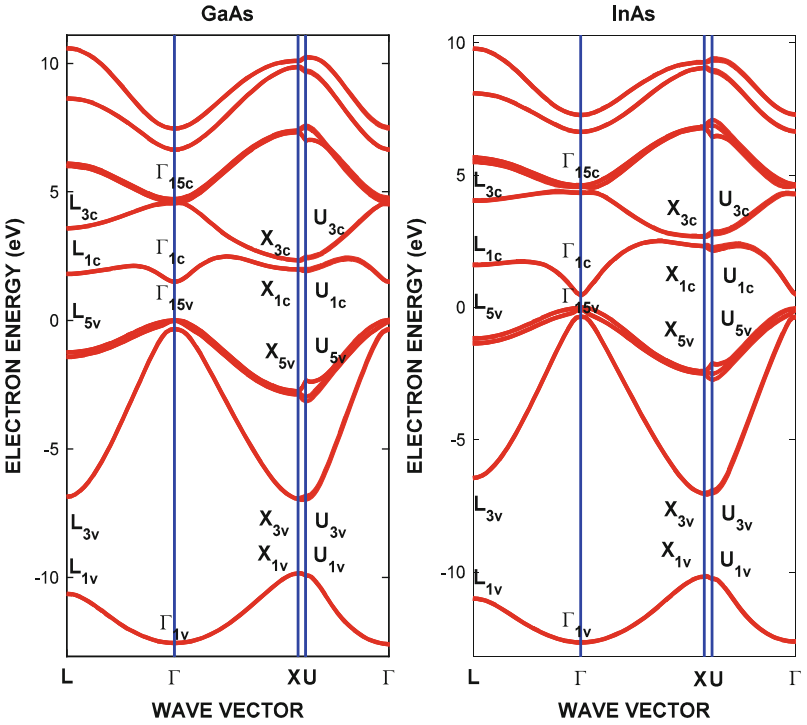

Fig. 2.4 Energy band structures of GaAs and InAs bulk semiconductors along Γ − L and Γ − X directions, obtained by using the 2NN sp^3s^* TB orbital basis sets

heavy-hole band, light-hole band, and spin–orbit splitting bands, of GaAs and InAs. In obtaining Fig. 2.4, TB interaction parameters $4V_{s^*,p}$ and $4V_{p,s^*}$ were adjusted to fit the X bands, and the 2NN interaction parameters ε_{sx} and ε_{xy} were chosen to get a good fit to the L bands in reproducing the pseudopotential energy bands [27].

Figure 2.5a, b, and c display the results of the 2NN sp^3s^* TB model for the conduction band and valence band electronic structures of GaP, GaN and InN compounds. As shown in Figs. 2.4 and 2.5 for bulk GaAs, InAs, GaP, GaN, and InN, adding the excited s^* state to the sp^3 basis set on the cation and anion atoms, with the 2NN interactions and spin–orbit coupling of p-states, makes it possible to better simulate the conduction band structure of III–V compounds, reproducing the pseudopotential bands [27] and measured bandgaps [28–30] at high symmetry points of the energy dispersion curve, which cannot be performed with NN or 2NN sp^3 ETB models. We should point out that the accuracy of our 2NN sp^3s^* TB model calculations depends on a good description of the band structures of GaAs, InAs, GaP, GaN, and InN compounds by the pseudopotential theory and/or accuracy of the experimental data.

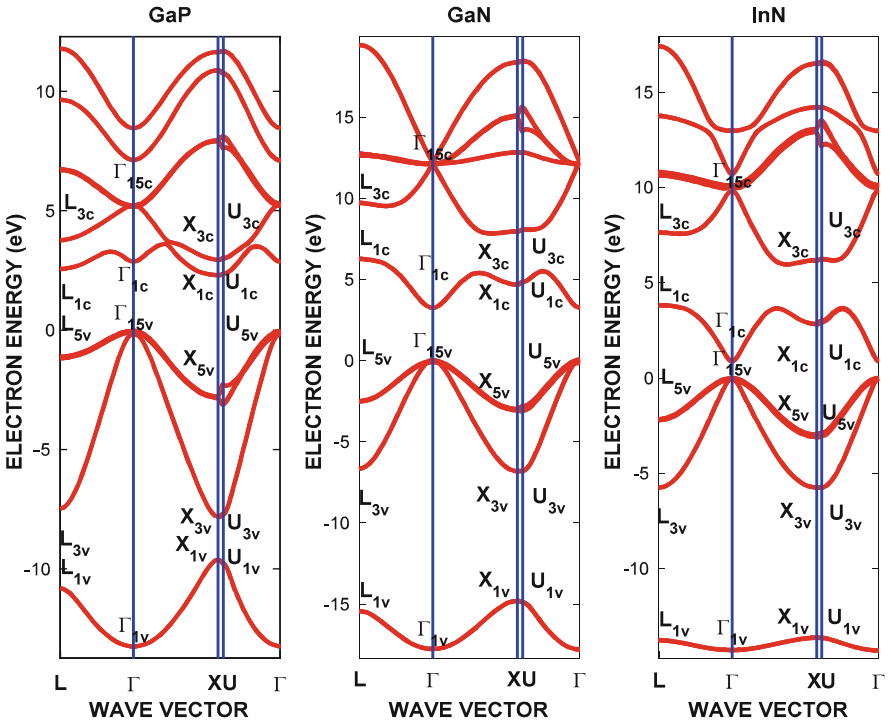

Fig. 2.5 Energy band structure of GaP, GaN, and InN compounds along $\Gamma - \mathrm{L}$ and $\Gamma - \mathrm{X}$ directions, obtained by using the 2NN sp^3s^* TB orbitals basis set listed in Table 2.2

2.4 Band Structure of Ternary Semiconductors

Within the framework of the 2NN sp^3s^* TB model, the effects of alloy composition and interface strain on the electronic band structure of heterostructures are calculated by using the so-called *modified virtual crystal approximation* (MVCA) [12–20]. The MVCA allows us to accurately take into account the disorder-induced nonlinear variation of the lattice constant and TB parameters in calculating electronic band structure properties such as bandgaps, conduction, and valence band offsets at the interface and, in turn, the effective masses of charge carriers. One first formulates the compositional dependence of bond length (or lattice constant) of ternary semiconductors ABC of an ABC/AC heterostructure written as the sum of undistorted bond length, $d_{\mathrm{VCA}} = (1-x)d^0_{\mathrm{AC}} + xd^0_{\mathrm{BC}}$, obtained by using the virtual crystal approximation (VCA), and the distortion in bond length, $d_{\mathrm{relax}} = x(1-x)\delta_{\mathrm{c}}(d_{\mathrm{BC}}(x) - d_{\mathrm{AC}}(x))$, due to cation–anion relaxation of binary in ternary [12–20]:

$$d(x) = d_{\mathrm{VCA}} + d_{\mathrm{relax}} = (1-x)d^0_{\mathrm{AC}} + xd^0_{\mathrm{BC}} + x(1-x)\delta_{\mathrm{c}}(d_{\mathrm{BC}}(x) - d_{\mathrm{AC}}(x)), \quad (2.19)$$

where $d_{AC}(x)$ and $d_{BC}(x)$ are the bond lengths of AC and BC binaries, respectively, in $A_{1-x}B_xC$ ternary:

$$d_{BC}(x) = (1-x)d^0_{AC} + xd^0_{BC} + (1-x)\xi_{BC:A}(d^0_{BC} - d^0_{AC}), \tag{2.20}$$

$$d_{AC}(x) = (1-x)d^0_{AC} + xd^0_{BC} + x\xi_{AC:B}(d^0_{AC} - d^0_{BC}) \tag{2.21}$$

where d^0_{AC} and d^0_{BC} are the undistorted bond lengths of host materials AC and BC. δ_c in (2.19) is the difference between two dimensionless relaxation parameters $\xi_{BC:A}$ and $\xi_{AC:B}$ [31].

$$\delta_c = \xi_{AC:B} - \xi_{BC:A} = \frac{1}{1 + \frac{\alpha_{AC}}{6\alpha_{BC}}\left(1 + 10\frac{\beta_{AC}}{\alpha_{AC}}\right)} - \frac{1}{1 + \frac{\alpha_{BC}}{6\varepsilon_{AC}}\left(1 + 10\frac{\beta_{BC}}{\alpha_{BC}}\right)}. \tag{2.22}$$

The effect of compositional disorder on the 2NN sp^3s^* TB Hamiltonian matrix elements is then described in terms of the host bond length and the distorted bond length by the substitutional impurity without any adjustable parameter [12–20]. The diagonal elements in the 2NN sp^3s^* TB Hamiltonian matrix for an $A_{1-x}B_xC$ ternary semiconductor are expressed as a nonlinear function of composition [12–20]:

$$E_{\alpha/\beta}(x) = (1-x)E_{\alpha/\beta}(AC) + xE_{\alpha/\beta}(BC) + x(1-x)\delta_c \Delta E_{\alpha/\beta}, \tag{2.23}$$

where $\Delta E_{\alpha/\beta} = E_{\alpha/\beta}(AC) - E_{\alpha/\beta}(BC)$, with α and β representing the fitted energies of the s, p, and s^* states of anion and cation atoms forming the AC and BC bulk semiconductors. The optimized TB parameters given in Table 2.2 are used in the calculations of the electronic structures of bulk GaPN, InAsN, and GaAsN nitride ternaries in k-space for various ternary alloy compositions, displayed in Fig 2.6a, b, and c showing the expected trend in band structures.

Note that there is a considerable lattice mismatch across ternary/binary heterointerfaces. Interface strain due to lattice mismatch causes a shift in the lattice constant of the epilayer: $a = (1+\varepsilon)a_0$, where ε is the symmetric strain tensor. Therefore, the bond lengths and off-site TB matrix elements are modified with strain. Consequently, the electronic properties of heterostructure constituents will be modified with respect to their unstrained values. The off-site TB matrix elements representing the NN interactions, known as the hopping strength, are correspondingly modified with respect to their unstrained values and are often determined by assuming that they obey the Harrison scaling law [26]: $V^s_{ll'm} = V_{ll'm}(a/a_0)^{-\eta_{llm}}$, where $V^s_{ll'm}$ is the strained and $V_{ll'm}$ the unstrained values of interaction potentials for anion and cation atoms. The exponents η_{llm} are determined so as to reproduce the strain variations of the band structure of relevant semiconductors under hydrostatic pressure, namely, the volume deformation potential $a_{gl} = -B(\partial E_{gl}/\partial P)$ for the corresponding bandgap energies at Γ, L, and X high symmetry points, which depend on the experimental values. This suggests that in order to obtain reliable and accurate TB parameters, one must go through a difficult fitting process that depends on the mapping of a large number of orbital coupling parameters on the set of observables

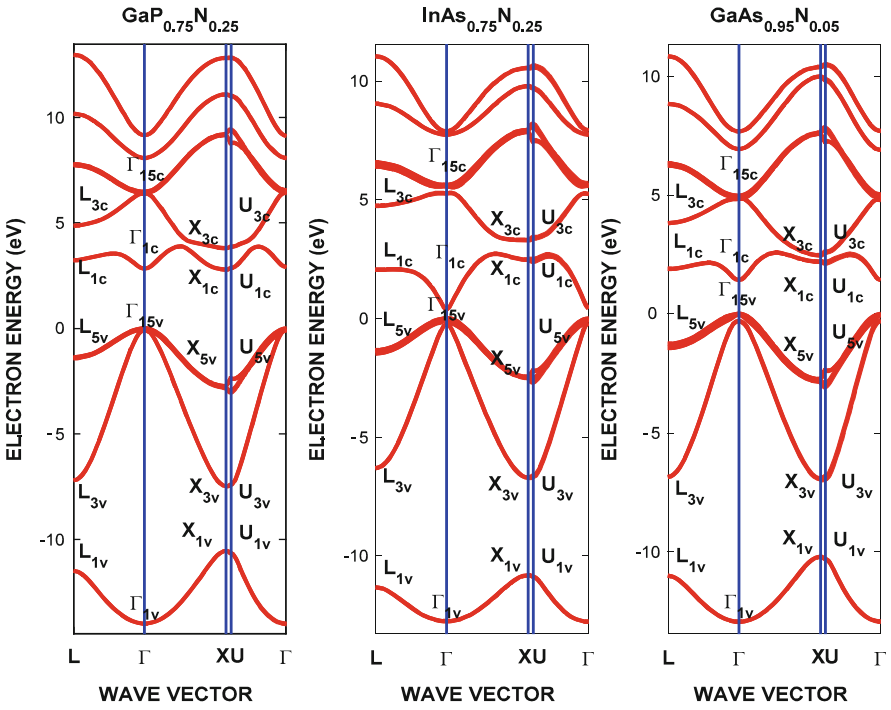

Fig. 2.6 Electronic band structures of GaPN (*left*), InAsN (*middle*), and GaAsN (*right*) bulk nitride semiconductors obtained by using 2NN sp^3s^* TB orbitals basis sets

and, in many cases, there are not many analytical expressions available. In such a process, an accurate and reliable determination of the strain effects on the energy levels by fitting the off-site TB matrix elements to set of observables is difficult. One can overcome this difficulty by using the statistical thermodynamic model [32] to study the interface strain effects on the electronic structure of heterostructure at symmetry points.

In determining the effects of interface strain on the energy band structures of heterostructures within the so-called statistical thermodynamic model of semiconductors [32], in which the conduction electrons and valence holes are treated as electrically charged chemical particles, one first expresses the shifts in the conduction and valence band edges at the Γ, L and X high symmetry points obtained by using the 2NN sp^3s^* TB orbitals basis sets as given by (2.7), (2.8) and (2.9). One then writes the shifts in the conduction and valence band energy levels and consequently, the bandgap energies of the heterojunction constituents as a function of temperature and pressure as

$$E_{ci}(T,P) = E_{ci} + C^{0}_{ciP}T(1-1nT) - \frac{a_{ci}}{B}\left[P - \frac{P^2}{2B} - \frac{(1+B')P^3}{6B^2}\right], \quad (2.24)$$

$$E_{v}(T,P) = E_{v} + C^{0}_{vP}T(1-1nT) - \frac{a_{v}}{B}\left[P - \frac{P^2}{2B} - \frac{(1+B')P^3}{6B^2}\right], \quad (2.25)$$

where E_v is the top of valence band at $k = 0$ (Γ symmetry point) and $a_v = -B(\partial E_v/\partial P)$ is its deformation potential. The index i corresponds to the Γ, L, and X symmetry points in the first Brillouin zone: $E_{c1} = E_{c\Gamma}$, E_{cL}, and E_{cX} are the conduction band minima at the Γ, L, and X symmetry points with deformation potentials $a_{c\Gamma} = -B(\partial E_{c\Gamma}/\partial P)$, $a_{cL} = -B(\partial E_{cL}/\partial P)$, and $a_{cX} = -B(\partial E_{cX}/\partial P)$.$B$ is the bulk modulus and $B' = \partial B/\partial P$ is its pressure derivative. $C^{O}_{cP} = C^{o}_{nP} - C^{O}_{oP} = -C^{o}_{pP} + \Delta C^{O}_{P}$ and $C^{o}_{vP} = C^{o}_{pP}$ are the standard state heat capacities of electron in conduction band valley E_{ci} and that of the valence hole at the top of the valence band energy E_v at constant pressure, with $\Delta C^{O}_{P} = C^{O}_{cP} + C^{o}_{vP} = C^{o}_{nP} + C^{o}_{pP} - C^{O}_{oP}$ as the change in the standard heat capacity of reaction. $C^{o}_{nP} = C^{o}_{pP} = (5/2)k_B$ for bare electrons and holes, k_B is the Boltzmann's constant.

Figure 2.6a, b, and c displays the lowest bandgap energies at the Γ, L, and X high symmetry points of the GaPN (left), InAsN (middle), and GaAsN (right) nitride-based ternary alloy components of GaAsN/GaAs, InAsN/InN and GaPN/GaP heterostructures. These figures clearly indicate that interface strain effects on the bandgaps points can be quite large when the bandgap deformation potential is large. As one can see from Fig. 2.7a, b, and c, the predicted principal bandgaps of nitride-based ternary alloys at Γ, L, and X high symmetry points, especially at Γ, are in excellent agreement with experimental data [28–30]. The bandgaps of the GaPN, InAsN, and GaAsN nitride-based ternary semiconductors first decrease with alloy composition (for N composition) roughly 25%, showing a negative slope, and increase gradually with alloy composition, having a large positive slope, in close agreement with experiments carried out on these materials. This observation suggests that by using the optimized 2NN sp^3s^* TB parameters for bulk GaAs, GaN, InAs, and GaP binary compounds, given in Table 2.2, the 2NN sp^3s^* TB model allows one to determine the nonlinear composition dependence of principal bandgaps of nitride-based ternary semiconductors without any empirical fitting and/or any adjustable parameters. This conclusion suggests that the 2NN sp^3s^* TB model can be a useful design tool for electronic and optoelectronic devices.

A comparison of predictions with experimental bandgap data for nitride ternaries, shown in Figs. 2.6, indicates that the proposed form of the 2NN sp^3s^* TB model predicts that the fundamental bandgaps of ternary semiconductors vary with alloy composition as

$$\begin{aligned} E_{gl}(x) &= (1-x)E_{gl\mathrm{AC}} + xE_{gl\mathrm{BC}} - \Delta E(x), \\ \Delta E(x) &= x(1-x)[E_{gl}(AC) - E_{gl}(BC)_l], \end{aligned} \quad (2.26)$$

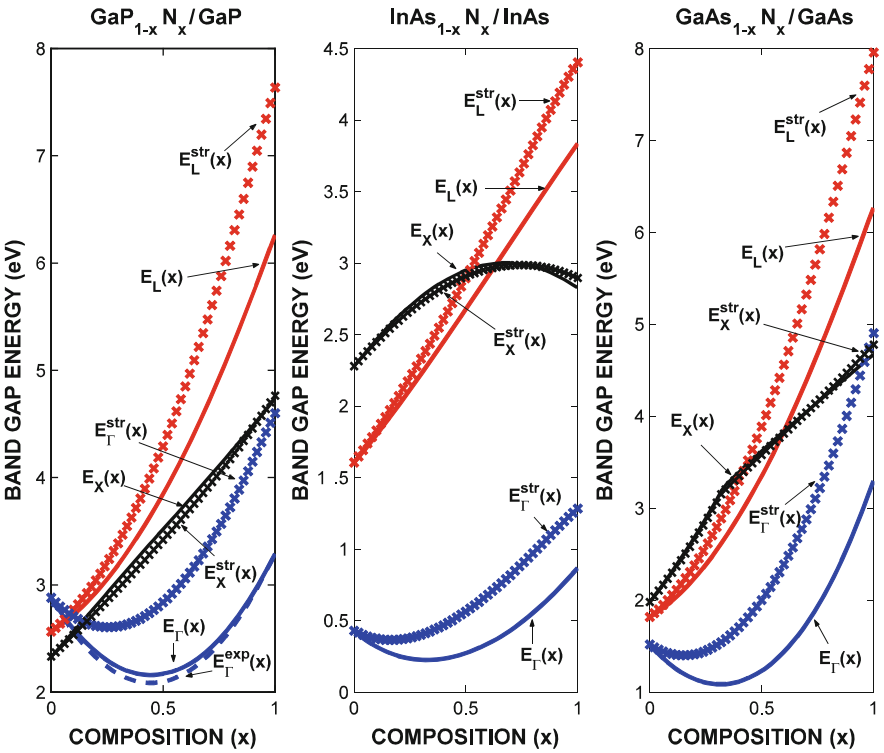

Fig. 2.7 Fundamental bandgaps of ternaries in GaPN/GaP (*left*), InAsN/InAs (*middle*), and GaAsN/GaAs (*right*) heterostructures calculated using the 2NN sp^3s^* TB orbitals basis set

where $\Delta E(x)$ represents the nonlinear effects of alloy composition on the fundamental bandgap energies of ternary semiconductors. Bandgap energies of GaPN, InAsN, and GaAsN appear to have positive bowing over the entire alloy composition range ($0 \leq x \leq 1$).

2.5 Band Offsets in Ternary/Binary Structures

The key feature involved in understanding the impact of nitride-based ternary/binary low-dimensional semiconductor structures on the performance of electronic and optical devices is the effect of alloy composition and strain variation on their energy band structure across the interface. Conduction and valence band offsets across the interface, shown in Fig. 2.8, control the electronic properties of heterostructure devices. In the context of the 2NN sp^3s^* TB model, the valence band offset across an ABC/AC ternary/binary heterostructure can be obtained by taking the difference between the valence band energies of the constituent bulk semiconductors screened

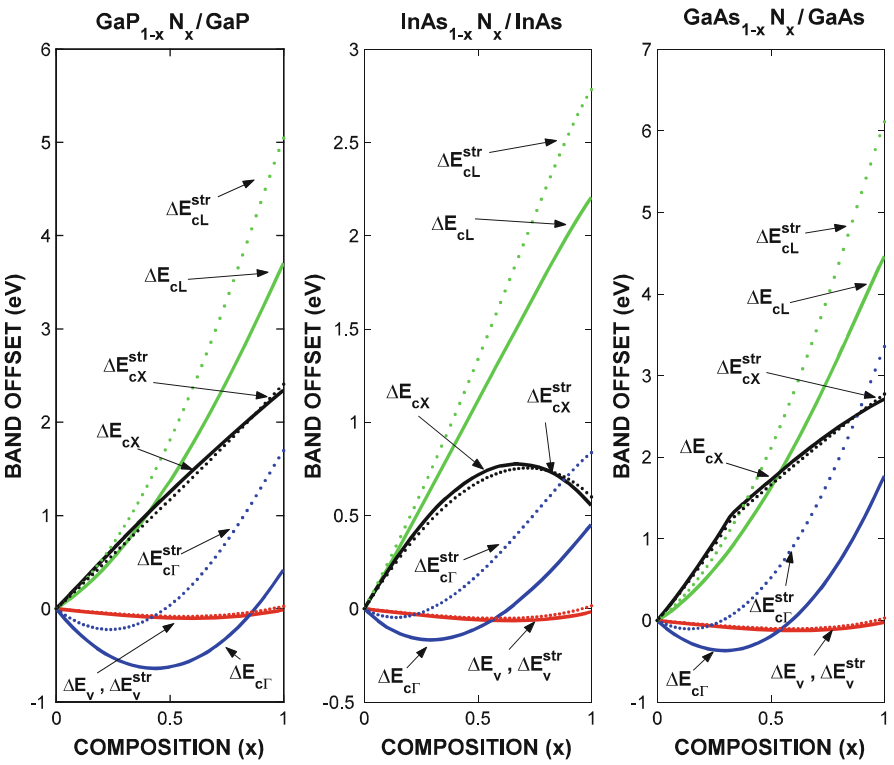

Fig. 2.8 Valence and conduction band offsets of GaPN/GaP (*left*), InAsN/InAs (*middle*), and GaAsN/GaAs (*right*) heterostructures calculated using the 2NN sp^3s^* TB model

with their optical dielectric constant, and then the conduction band offset for a given Γ, L, and X high symmetry point of the Brillouin zone is given as the difference between the bandgap difference, written as [32]:

$$\begin{aligned} \Delta E_{\mathrm{v}} &= \left(\frac{E_{\mathrm{v}}}{\varepsilon_{\infty}}\right)_{\mathrm{BC}} - \left(\frac{E_{\mathrm{v}}}{\varepsilon_{\infty}}\right)_{\mathrm{ABC}}, \\ \Delta E_{ci} &= E_{ci\,\mathrm{ABC}} - E_{ci\,\mathrm{BC}} = \Delta E_{gi} - \Delta E_{\mathrm{v}}, \end{aligned} \tag{2.27}$$

where $E_{\mathrm{v}} = E_{\mathrm{v}}(\Gamma_{15})$ is the top of the valence band at the Γ high symmetry point and $E_{ci} = E_{\Gamma_{6c}}, E_{L_{6c}}$, and $E_{X_{6c}}$ are the bottom of the conduction bands at the Γ, L, and X high symmetry points, determined with the proposed form of the 2NN sp^3s^* TB model discussed in "TB View of Semiconductor Structures" section using the optimized TB parameters listed in Table 2.2. Here, $\Delta E_{gi} = E_{gi}(\mathrm{ABC}) - E_{gi}(\mathrm{BC})$ is the difference between bandgaps of the bulk ABC ternary and BC binary compound semiconductors with bandgaps $E_{gi}(\mathrm{ABC})$ and $E_{gi}(\mathrm{BC})$, where $E_{gi} = E_{g\Gamma}, E_{g\mathrm{L}}$, and $E_{g\mathrm{X}}$ are the principal bandgaps at the Γ, L, and X

symmetry points. ε_∞(ABC) and ε_∞(BC) are the optical dielectric constants of bulk ABC ternary and BC binary semiconductors. The band offsets in III–V nitride-based ternary/binary heterostructures are shown in Fig. 2.7 for GaPN/GaP (left), InAsN/InAs (middle), and GaAsN/GaAs (right) as a function of interface strain for the entire composition range ($0 \leq x \leq 1$).

As shown in Fig. 2.8, the interface strain effect on the valence band offsets in the GaPN/GaP, InAsN/InAs, and GaAsN/GaAs nitride-based heterostructures is rather small because of the smaller valence band deformation potentials. However, the interface strain effects on conduction band offsets at Γ, L, and X high symmetry points can be quite large because of the large conduction band deformation potentials. Furthermore, the conduction band offset of the InAsN/InAs structure at the X high symmetry point has a negative slope and is fairly nonlinear with composition. When we analyze the compositional variations of conduction band offsets at the Γ high symmetry point of the first Brillouin zone, we note that they are mostly negative at lower compositions $0.0 < x < 0.50$ and become positive for larger compositions, $0.50 < x < 1$. We can say that GaPN/GaP, InAsN/InAs, and GaAsN/GaAs nitride-based heterointerfaces are type II for smaller alloy compositions ($0.0 < x < 0.50$) and become type I as the alloy composition increases ($0.50 < x < 1.0$).

2.6 Semiempirical $sp^3d^5s^*$ TB Model

From comparison of electronic band structures calculated with pseudopotential theory and sp^3 and sp^3s^* ETB models, Jancu et al. [21] realized that the excited d-states make a critical contribution to both the valence band maximum at the Γ high symmetry point and to the conduction band dispersion curves at the X and L symmetry points; and he developed an NN$sp^3d^5s^*$ semiempirical TB model with NN interactions to calculate the electronic band structure of group IV and III–V semiconductors. The valence band and conduction band dispersion curves obtained with the NN$sp^3d^5s^*$ model are found to overcome most of the limitations of the earlier TB models. This accurate description of the second conduction band and the transverse effective masses at the X- and L-symmetry points are found to be in good agreement with experimental data, leading to a reliable TB model for the calculation of the optical properties involving high symmetry points at the edge of the first Brillouin zone of tetrahedral semiconductors. Figure 2.9 shows the comparison of the electronic band structure and DOS of GaAs calculated using the 2NN sp^3s^* and NN $sp^3d^5s^*$ TB methods. Correspondingly, Fig. 2.10 exhibits the band structure and DOS of GaN calculated using the NN $sp^3d^5s^*$ TB method [21] and DFT [22].

In the framework of the NN $sp^3d^5s^*$ TB models, the effects of alloy composition on the electronic band structure of ternary/binary heterostructures are calculated using MVCA [14–16,20]. This MVCA approximation makes it possible to calculate the disorder nonlinear variation of the lattice constant and TB parameters in the determination of the electronic structure properties (such as bandgaps and band

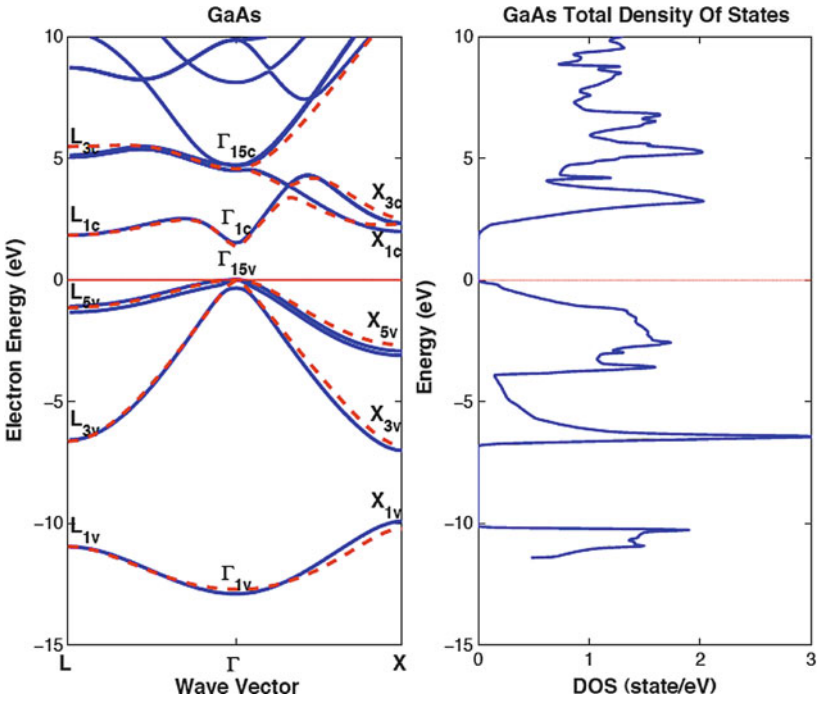

Fig. 2.9 Electronic band structure and DOS of GaAs calculated using the 2NN sp^3s^* (*dashed*) and NN $sp^3d^5s^*$ (*solid*) TB methods

offsets as shown in Fig. 2.11 for AlGaAs/GaAs heterostructures at 300 K) from fundamental bandgap energy and conduction and valence band offsets compared in Fig. 2.11 with results of DFT calculations carried out by our group and experiment.

2.7 Conclusion

The realization of the full potential of low-dimensional semiconductor structures for electronic device technologies requires a reliable and precise predictive process and performance simulation models that are consistent with the fundamental principles of solid-state physics and quantum mechanics. The use of low-dimensional semiconductor structures in device design allows the device engineer to locally modify the energy band structure of the constituents in order to control the motion of charge carriers. When two semiconductors with different physical and chemical properties and thicknesses are grown upon each other, the lattice mismatch and thermal expansion gradient over the growth temperature causes interface strain that modifies the electronic properties of both materials, including the band offsets, and consequently, the energy of the moving charge carriers at the conduction and

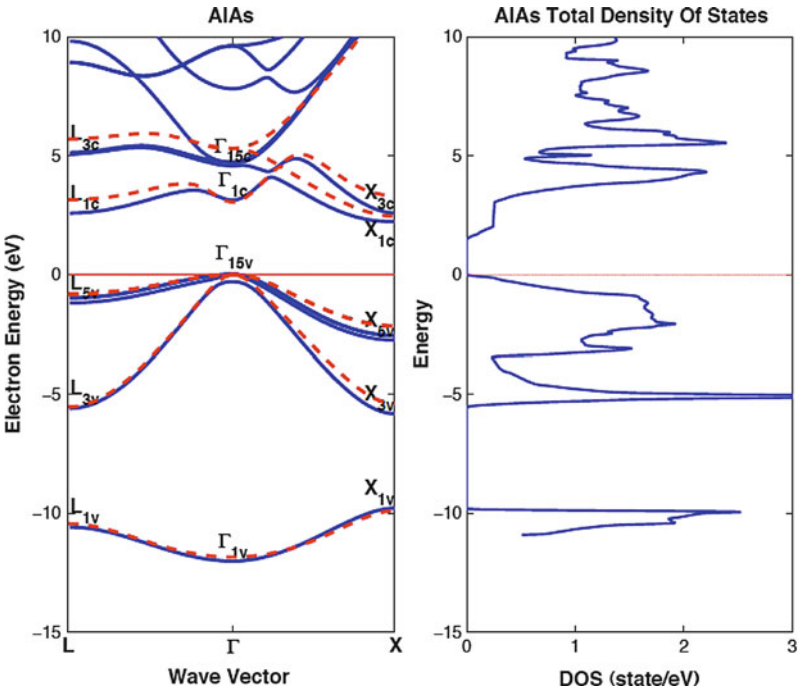

Fig. 2.10 Electronic band structure and DOS of AlAs calculated using the NN $sp^3d^5s^*$ TB method (*solid*) and DFT (*dashed*)

valence band edges must change across the heterointerface, influencing the device performance. Key issues involved are understanding the formation and determining the magnitude of the conduction and valence band offsets at the interfaces of low-dimensional structures, which dominate various device properties and has received considerable attention among the device scientists and engineers over the years.

In this chapter, we presented a general methodology for a qualitatively reliable and quantitatively precise calculation of the electronic band structure of low-dimensional semiconductor heterostructures. The models discussed in this chapter include the semiempirical sp^3 TB theory and DFT of band structure modeling, which can be implemented very easily in current transport modeling for low-dimensional semiconductor structures to insure accurate design and simulation of electronic and optoelectronic devices.

Acknowledgements This work was partially supported by the Scientific and Technical Research Council of Turkey (TÜBİTAK) under Grant No: TBAG-105T463. Two of us, H. H. Gürel and Ö. Akıncı, greatly acknowledge the Ph.D. student fellowships by Turkish State Planning Agency (DPT). The authors would like to greatly acknowledge the computer usage of High Performance Computing Laboratory of Informatics Institute at stanbul Technical University.

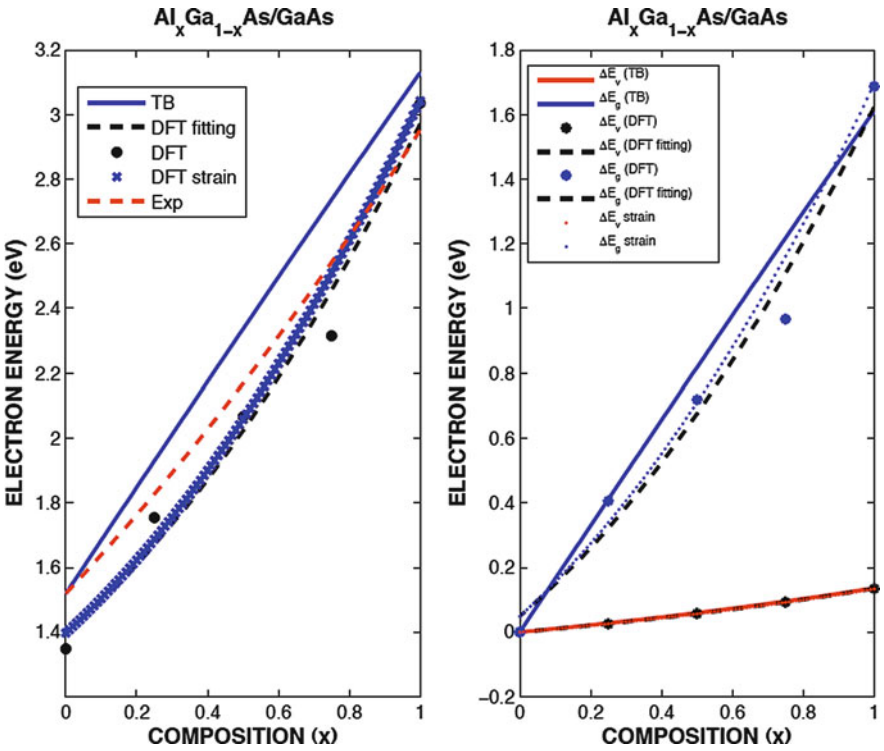

Fig. 2.11 Composition effects on bandgaps and band offsets in an AlGaAs/GaAs heterostructure calculated using the NN $sp^3d^5s^*$ TB method (*solid*) and DFT (*dashed*)

References

1. H. Morkoç, H. Ünlü, G. Ji, *Principles and Technology of MODFETs*, vols. 1, 2 (Wiley, Chichester, 1991)
2. B. Gil (ed.), *Group III Nitride Semiconductors Compounds: Physics and Applilcations* (Oxford Science Publications, Oxford, 1998)
3. H. Ünlü, H. Morkoç, Solid State Technol. **31**, 83 (1988).
4. H. Morkoç, H.Ünlü, in *Semiconductors and Semimetals*, vol. 24, ed. by R. Dingle (1987), p. 135, (Academic Press, 1987)
5. H. Ünlü, H. Morkoç, S. Iyer, in *Gallium Arsenide Technology*, vol. 2, ed. by D.K. Ferry (1990), p. 231, (Howard & Sams, 1990)
6. H. Morkoç, H.Ünlü, H. Zabel, N. Otsuka, Solid State Technol. **31**, 71 (1988)
7. H. Kroemer, Proc. IRE **45**, 1535 (1957)
8. H. Kroemer, Proc. IEEE **70**, 13 (1982)
9. J.-M. Jancu et al., Phys. Rev. B **57**, 6493 (1998)
10. A. Di Carlo, Semicond. Sci. Technol. **18**, R1 (2003)
11. G.L. Bir, G.E. Pikus, *Symmetry and Strain – Induced Effects in Semiconductors* (Wiley, New York, 1974).
12. H. Ünlü, Phys. Status Solidi (B) **216**, 107 (1999)
13. Ö. Akıncı, H.H. Gürel, H. Ünlü, Thin Solid Films **517**, 2431 (2009)

14. H.H. Gürel, Ö. Akıncı, H. Ünlü, Thin Solid Films **516**, 7098 (2008)
15. Ö. Akıncı, H.H. Gürel, H. Ünlü, Phys. Status Solidi (C) **5**(2), 478 (2008)
16. Ö. Akıncı, H.H. Gürel, H. Ünlü, J. Nanosci. Nanotechnol. **8**, 540 (2008)
17. H.H. Gürel, Ö. Akıncı, H. Ünlü, Phys. Status Solidi (C) **4**(2), 316 (2007)
18. H.H. Gürel, Ö. Akıncı, H. Ünlü, Superlattices Microstruct **40**(4–6), 588 (2006)
19. Ö. Akıncı, H.H. Gürel, H. Ünlü, Thin Solid Films **511–512**, 684 (2006)
20. H.H. Gürel, Ö. Akıncı, H. Ünlü, Comput. Mater. Sci. **33**, 269 (2005)
21. P. Vogl, H.P. Hjalmarson, J.D. Dow, J. Chem. Solids **44**, 365 (1983)
22. J.-M. Jancu et al., Phys. Rev. B **57**, 6493 (1998)
23. J.-M. Jancu et al., Appl. Phys. Lett. **81**, 4838 (2002)
24. J.C. Slater, G.F. Koster, Phys. Rev. **94**, 1498 (1954)
25. D.J. Chadi, M.L. Cohen, Phys. Status Solidi **68**, 405 (1975)
26. W.A. Harrison, *Elementary Electronic Structure* (World Scientific, Singapore, 1999)
27. M.L. Cohen, J.R. Chelikowsky, *Electronic Structure and Optical Properties of Semiconductors*, 2nd edn. (Springer, Berlin, 1989)
28. O. Madelung (ed.), *Numerical Data and Functional Relationships in Science and Technology*, vol. 17a (Springer, Berlin, 1982)
29. O. Madelung (ed.), *Numerical Data and Functional Relationships in Science and Technology*, Part a of vol. 17 (Springer, Berlin, 1982) and Part d of Vol. 17 (1984)
30. I. Vurgaftman, J.R. Meyer, L.R. Ram-Mohan, J. Appl. Phys. **89**(11), 5815 (2001)
31. J.L. Martins, A. Zunger, Phys. Rev. B **30**, 6217 (1984)
32. H. Ünlü, Solid State Electron. **35**, 1343 (1992)

http://www.springer.com/978-3-642-28423-6

Low Dimensional Semiconductor Structures
Characterization, Modeling and Applications
Ünlü, H.; Horing, N.J.M. (Eds.)
2013, XIV, 162 p., Hardcover
ISBN: 978-3-642-28423-6